Hindawi Publishing Corporation
International Journal of Polymer Science
Volume 2016, Article ID 4269039, 9 pages
http://dx.doi.org/10.1155/2016/4269039

Research Article

Effect of Elastomeric Nanoparticles on Polystyrene/Organic Nanocomposites

Sungwon Ma and Yonathan Thio

School of Polymer, Textile and Fiber Engineering, Georgia Institute of Technology, 801 Ferst Dr. NW, MRDC 1, Atlanta, GA 30332-0295, USA

Correspondence should be addressed to Sungwon Ma; sungwma@gmail.com

Received 4 July 2016; Accepted 31 August 2016

Academic Editor: Ehsan Bafekrpour

The rheological behavior of nanosheet composites and the effect of morphology between elastomeric nanofiber and nanosheet composites were studied using a Cross-Williamson model and critical volume concentration was investigated by percolation threshold theory for fiber and sheet morphologies. Nanofiber and nanosheet particles were synthesized by a cold vulcanization process using a S_2Cl_2 cross-linking reagent resulting from self-assembly of a PS-PI block copolymer. Nanofiber and nanosheet characterization was done by SEM. Rheological properties were measured and analyzed in terms of varying nanofiller and nanosheet loading from 0.5 to 10 wt%. For the nanofiber and nanosheet composites, the moduli were increased with increasing filler loading, whereas moduli of SI23 and SI43 composite decreased with increasing content. Both nanofiber and nanosheet composites showed a nanosized filler effect and their structural changes were between 5 and 10 wt%. Cross-Williamson three-parameter model was used to find zero-shear viscosity and relaxation time. Percolation threshold theory was used to study structural changes and calculate values.

1. Introduction

Polymer nanocomposites have drawn much attention over the last several decades in terms of both research interest and industrial [1–3] applications that involve optical [4, 5], biomedical [6], electrical [7–9], and reinforcing properties [10–13]. Many studies have been done in order to understand their morphologies [14] and mechanical behavior [15, 16]. In addition, polymer nanocomposite studies have focused on critical factors such as nanoparticle/matrix interaction, nanoparticle shape, and size [1, 11].

Polymer nanocomposites have been studied to better understand their toughening mechanism using an elastomer modified epoxy as exemplified in recent reviews and articles by Mangaraj, Rajeev, and Yee [16–18]. Lee and Goettler [13] also explored composite structure-property relationships. In addition, many studies have looked at CNT, clay, and $CaCO_3$ as inorganic fillers in polymer nanocomposite [12, 19, 20]. However, the elasticity of the composite decreases with an increasing amount of inorganic nanofiller. This property would be a limitation for film applications that require both flexibility and gas barrier property. To the best of our knowledge, there have been no previous detailed studies looking at composites with elastomeric nanoparticles having cylindrical and sheet morphologies using block copolymer self-assembly technique and cold vulcanization process. Many studies have looked at rubber toughening properties via a spherical shape. In a rubber blend, rubber particles are generated as spherical shapes measuring several micrometers in diameter to reduce surface tension.

In this paper, we studied the rheological behavior of elastomeric nanofiber and nanosheet composites. The particles can be generated by a self-assembly technique and cold vulcanization process using an elastomeric PS-PI block copolymer. The block copolymer self-assembly property is one useful technique for controlling the nanoscaled morphologies of particle shapes such as a sphere, cylinder, and lamellar. Many papers have been published regarding potential applications of block copolymers [1, 21]. Most of the studies focused on the interaction and morphology between matrix and inorganic nanoparticles.

Table 1: Characterization data of PS-b-PI copolymers. Volume fractions of polyisoprene were calculated from specific volumes of PS and PI [25, 26].

Polymer	Mn (g/mol)	T_g (°C)$_{DSC}$		PDI	PI content	Morphology
	PS-*b*-PI	PS part	PI part	M_w/M_n	Vol. fraction	
SI23	23-*b*-8.0	101.69	−68.95	1.07	0.23	Cylinder
SI43	31.6-*b*-28	91.42	−62.37	1.06	0.43	Lamellar

Our approach is to use the block copolymer itself as the elastomeric nanoparticle. In the bulk state, a block copolymer can be self-assembled by controlling volume fraction, molecular structure, and molecular weight. Thus, control of these factors would be a facile method to obtain desired spherical, cylindrical, and lamellar morphologies. However, when a PS-PI block copolymer is blended with PS, the composite morphology may be changed by the total volume fraction of PS. Thus, a cold vulcanization process is used in order to generate the desired morphology without changing the structure when it is mixed.

The cold vulcanization process was first used by Glazer [22] who utilized a sulfur compound (S_2Cl_2) to understand the kinetics of this vulcanization process. Recently, the process was used to prepare nanofibers using a PS-PI block copolymer having a cylindrical morphology as published by Liu et al. [23]. Additionally, the author also studied the properties of a PS-PI nanofiber in terms of cross-link density [24].

In this paper, elastomeric PS-PI nanofiber and nanosheet were prepared and characterized. Using rheological behavior, critical volume fraction was investigated through three parameters of a Cross-Williamson model and thru percolation threshold theory. We found that the moduli increased with increasing nanofiber and nanosheet loading, and the critical volume fraction of the nanosheet was found and compared with nanofiber in the composite.

2. Experimental

2.1. Materials. Polystyrene-b-polyisoprene copolymers were obtained from Polymer Source Co. Ltd. whose characteristics are listed in Table 1. Sulfur chloride (S_2Cl_2) was purchased from Aldrich and commercially available polystyrene of $\overline{M}_w$ = 350,000 g/mol (PDI: 2.06) was also purchased from Aldrich. The materials and solvents were used as received without any purification.

2.2. Preparation of Nanofiber and Nanosheet. Nanofiber and nanosheet synthesis was done using a modification method by Liu et al. [23] 1 g of a PS-b-PI copolymer dissolved in toluene with vigorous stirring. After the block copolymer was completely dissolved, the solution was dried in a glass dish under a nitrogen condition for three days. The dried sample was exposed to S_2Cl_2, which was cross-linking agent, for a week. The cross-linked sample was swelled using THF for a week. Sonication and centrifugation were then used to separate highly cross-linked gel and nanoparticles. The separated samples were first precipitated in methanol and then the yellowish sample was filtered and dried in a vacuum oven for 24 hrs in order to remove residual solvent.

2.3. Preparation of Composite Sample. Blends of polystyrene and composites of nanoparticles were made using a solvent casting process in order to mix completely. PS of 5 g was dissolved in toluene with various weight percent of nanoparticles: 0.5, 1.0, 2.0, 5.0, and 10 wt%. The mixtures were poured into aluminum foil and dried for three days. The blends were further dried in a vacuum oven at 100°C for 12 hrs in order to remove residual toluene.

2.4. SEM. Nanofiber and nanosheet morphologies were imaged using a Scanning Electron Microscope (Model: LEO 1530). Gold coating was applied by gold sputter for all SEM samples. The images were obtained by thermally assisted field emission Scanning Electron Microscope applying 5 keV using the in-lens detector.

2.5. Rheology. The rheological properties of the composites were measured and analyzed by an AR2000 (TA instrument) using a parallel plate geometry of 25 mm diameter. All samples were tested at a temperature range from 160°C to 200°C with a 10°C step. All experiments were performed at a frequency range from 0.01 to 100 Hz. The gap distance and percent strain were 1000 μm and 0.05, respectively.

3. Results and Discussion

3.1. Characterization of Nanofiber and Nanosheet. Nanofiber and nanosheet were synthesized by cold vulcanization and a self-assembly technique of PS-b-PI copolymer. Cylindrical and lamellar morphologies of PS-b-PI were used as a form of fiber and sheet, individually. In general, PS and PI were maintained at volume fractions 77 and 23 resulting in a cylindrical form with a PS shell and PI core [23]. When a S_2Cl_2 cross-linking agent was applied to the cylinder morphology of the PS-b-PI sample, a double bond of polyisoprene started to form a linkage between backbone chains by generating sulfur bridges. Thus, the cross-linked core was able to maintain the cylindrical morphology as a fiber. For a nanosheet, similar process was applied and the only difference was that the volume fractions of PS and PI were 57 and 43, respectively. Figure 1 shows that nanofiber and nanosheet morphologies were clearly confirmed as nanofillers and individual nanofillers are shown in the inserted images. The diameter of a nanofiber and the thickness of a nanosheet were approximately 40 nm and 70 nm, respectively. The diameter and thickness of the nanofiller resulting from vulcanization of the

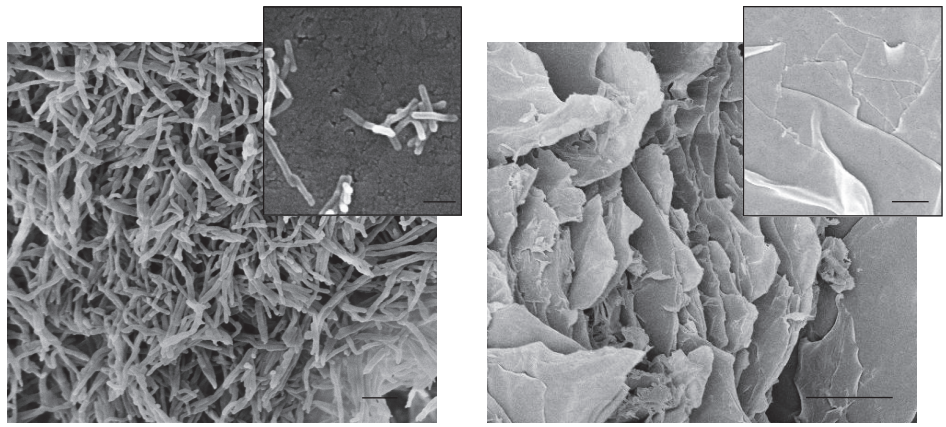

Figure 1: SEM image of nanofiber and nanosheet morphologies in bulk state. The inserted images are shown as a single nanofiber and nanosheet on a silicon wafer. The scale bars indicate 300 nm and 100 nm and 10 μm and 1 μm.

block copolymer strongly depend on the molecular weight of the PS-b-PI copolymer [27].

3.2. Rheological Properties. The rheological results at 180°C showed that the moduli of the composites increased with increasing nanofiber or nanosheet loading compared with the moduli of the blend of PS/SI23 and PS/SI43. In order to study a wider range of frequency, a master curve was applied.

The master curves of the samples are shown in Figure 2. Storage modulus versus frequency was plotted for the two nanofiller composites as shown in Figures 2(a) and 2(c). Two uncross-linked blends are shown and compared in Figures 2(b) and 2(d). The graphs showed that the storage modulus of nanofiber and nanosheet composites increased with increasing nanofiller content, whereas modulus of PS/SI23 and PS/SI43 blends had no significant increase with increasing SI23 or SI43 content. The differences came from cross-linking variation of isoprene units in nanofillers and block copolymers. Nanofiber and nanosheet maintained their structures in the composite because of a cross-linked isoprene unit. But SI23 or SI43 was not able to sustain their own morphology as cylinder or lamellar when blended with PS because the total volume fraction of PS increased. In Figures 2(a) and 2(c), the composite that included 10 wt% nanosheet had a slightly higher modulus value than the composite of 10 wt% nanofiber. The nanosheet more effectively prevented mobility of PS than nanofiber and this resulted from an approximately 2.5 times higher aspect ratio for the nanosheet. This result showed that the shape and geometry of the elastomeric nanofillers were an important factor for control of elastic modulus in a composite.

G'/ω and $\eta'(G''/\omega)$ versus angular frequency are presented in Figure 3. According to Sepehr et al. [28], the dynamic elasticity coefficient was expressed as $\psi = G'/\omega^2$ and the plot of $G'/\omega = \psi\omega$ versus ω gave information of the melt in terms of structural change. In addition, the plot of $\psi = G'/\omega^2$ versus ω showed very similar results of $\eta'(G''/\omega)$ versus ω, in nanofiber composites. Figure 3(a) indicated that there were three-dimensional structural changes around a 5 wt% loading. In the case of the nanosheet composites, the graphs showed similar results with the nanofiber composites. The slope variation at the low frequency range suggested that a new structure such as with a continuous domain or aggregation was generated around 5 wt% filler loading and was clearly distinguished based on slope change at a low frequency range. From the graphs, the slope changes of nanosheet composites were larger than the slope changes of nanofiber composites at low frequency ranges and the variation appears more gradually than the nanofiber composites. This suggested that the structural changes could be detected after 2 wt% nanofiber loading and then the nanofiber generated a three-dimensional structure such as percolation point. However, in the case of the nanosheet, the filler started to affect the structural change gradually from a low wt% of nanosheet loading because of a high aspect ratio and size.

In order to investigate the effect of relaxation, a Cole-Cole plot was applied [29]. Long relaxation behavior was also observed in the Cole-Cole plot by comparing the radius in a graph. The calculated Cole-Cole plot consisted of the imaginary part and real part in terms of the frequency dependent shear modulus that directly indicated stress relaxation time by changing the radius of the plotted data. In Figure 4, the Cole-Cole plots are shown by variation in nanofiller loading. As shown in the figure, the radius of each sample increases with increasing filler loading. In the plot of nanofiber composites, the radius increased dramatically between 2 wt% and 5 wt%. This suggested that a small loading of nanofiber was able to affect the relaxation time in a matrix PS molecule and there was detection of structural change between 2 wt% and 5 wt%. However, in the case of the nanosheet composite, the radius increased gradually until 2 wt% and then dramatically increased at 5 wt%. This indicated that the nanosheet was less effective than nanofiber below 2 wt% due to its morphology, but after 2 wt% the nanosheet is more effective than nanofiber in terms of retarding the relaxation process. The Cole-Cole plot showed the relaxation time variation per increasing nanofiller loading.

$\tan\delta$ provides another method to present the relaxation in the composite matrix [30, 31]. $\tan\delta$ is defined as the ratio of the loss modulus and storage modulus. From the Doi and

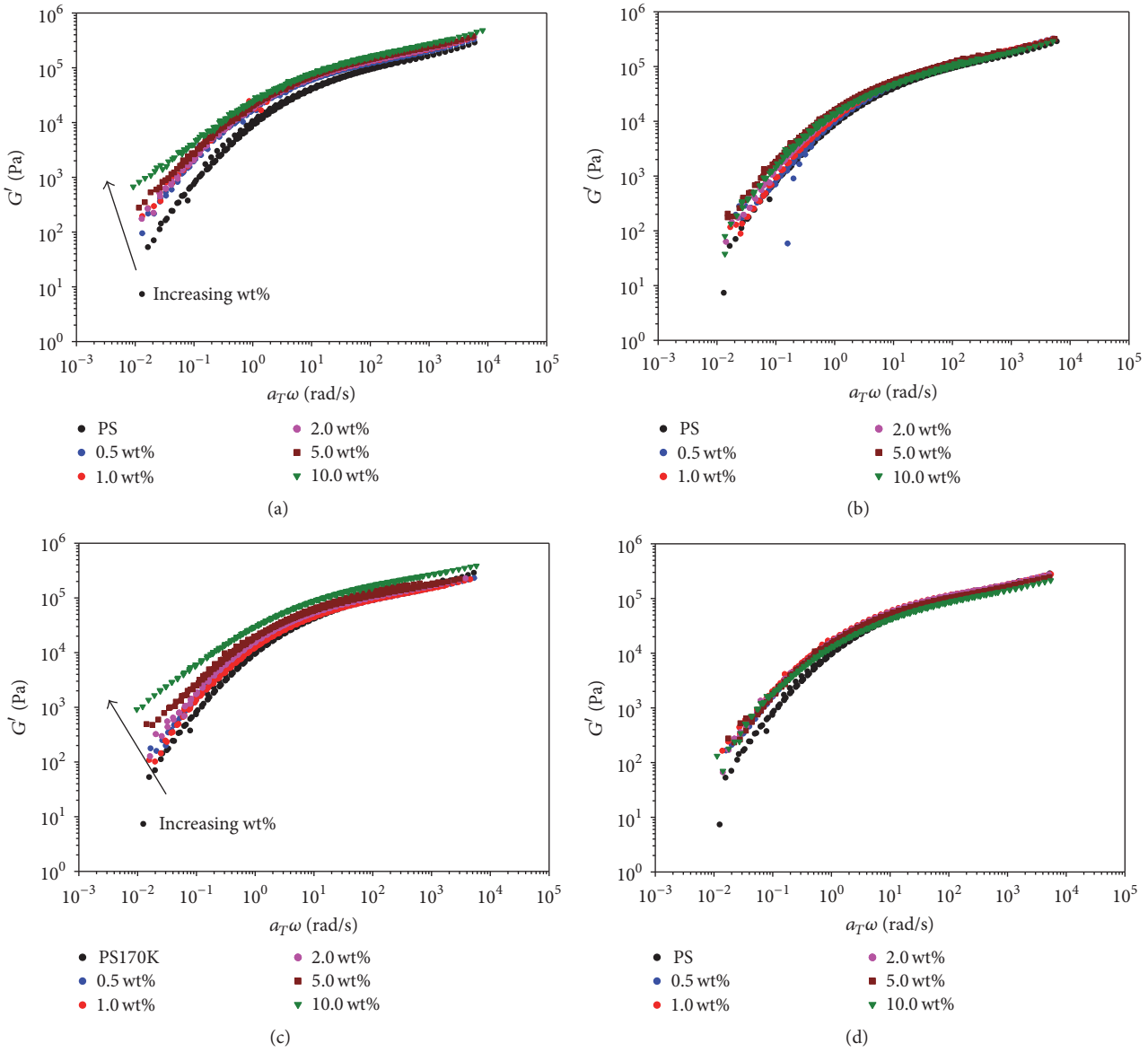

Figure 2: Master curve of storage modulus of (a) PS/nanofiber, (b) PS/SI23, (c) PS/nanosheet, and (d) PS/SI43 blend with varying weight fraction of fillers. The reference temperature is 180°C.

Edwards model [32], loss and storage moduli were expressed by an equation which was a combination of relaxation time and angular frequency. Thus, $\tan\delta$ can be expressed by

$$\tan\delta = \frac{G''}{G'} = \frac{\sum_p \left((1/p)\,\omega\tau_p / \left(1+\left(\omega\tau_p\right)^2\right)\right)}{\sum_p \left((1/p)\left(\omega\tau_p\right)^2 / \left(1+\left(\omega\tau_p\right)^2\right)\right)}, \quad (1)$$

where τ is relaxation time and ω is angular frequency. When $\omega \to 0$, this leads to a proportionality between $\tan\delta$ and ω^{-1}. And thus a log-log plot of $\tan\delta$ versus ω^{-1} should show a slope of -1 at low ω in polymer.

$\tan\delta$ versus angular frequency taking logarithm curves are plotted in Figures 5 and 6. Han et al. [25] found the relationship between $\log G'$ and $\log G''$ using a Doi-Edward tube model. In some cases, however, the slope was not matched to the value because of two reasons: one was not reached sufficiently at a low frequency for the terminal region and another was due to polydispersity. In our case, we found the relationship between $\log(\tan\delta)$ and $\log\omega$ as a value of -1 using the Doi-Edward tube model in PS. Figure 6 and Table 2 show that the value of slope increased with increasing filler

Table 2: Slope results of logarithm $\tan\delta$ plot with varying nanofiller loading. Slope of neat PS is −0.54.

Wt% of filler	0.5	1	2	5	10
Nanofiber (slope)	−0.57	−0.44	−0.43	−0.30	−0.09
Nanosheet (slope)	−0.48	−0.64	−0.46	−0.26	−0.19

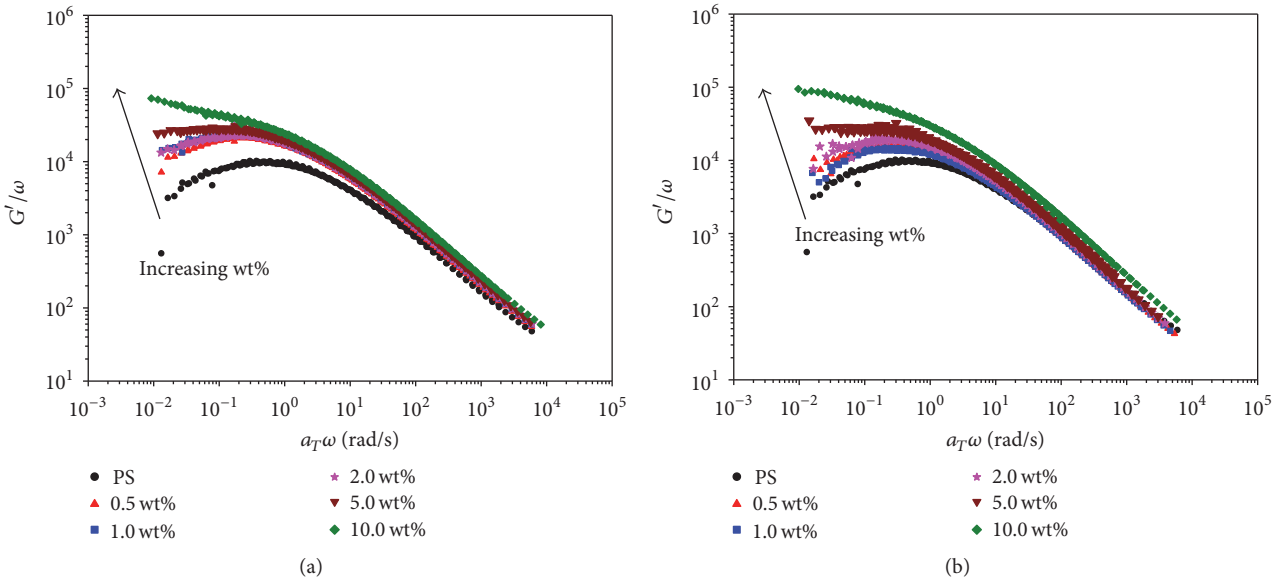

FIGURE 3: G'/ω versus angular frequencies was plotted using master curve. (a) Nanofiber/PS blend and (b) nanosheet/PS blend in terms of nanofiller loading.

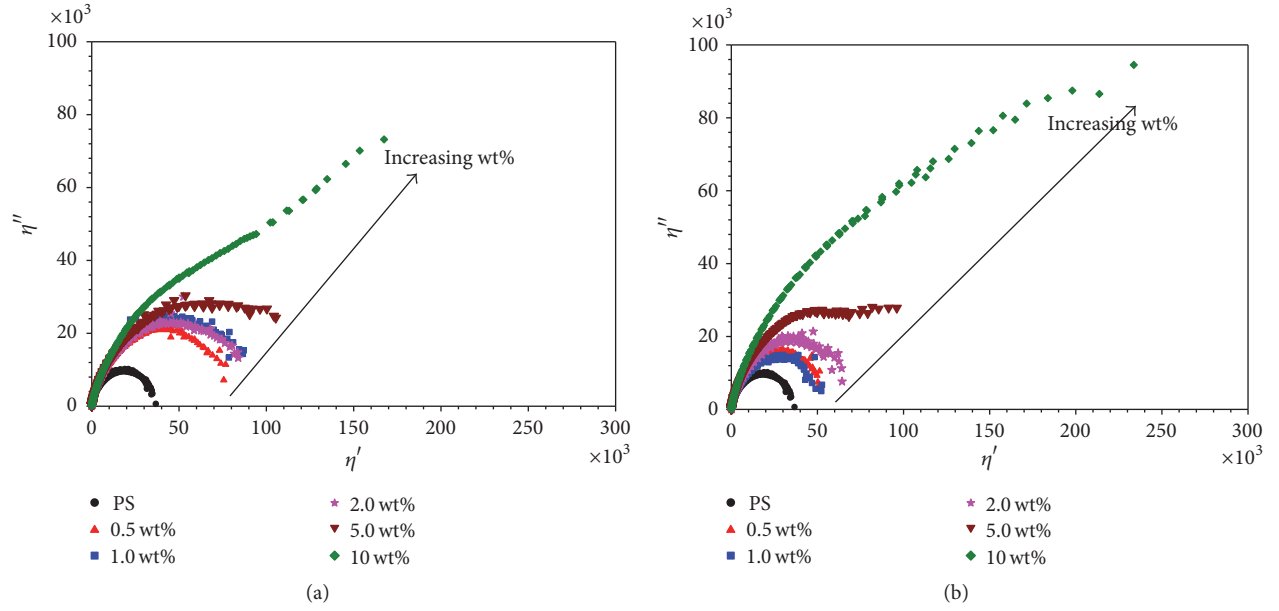

FIGURE 4: Cole-Cole plot (η'' versus η') of blend of neat PS with (a) PS/nanofiber and (b) PS/nanosheet using master curve.

loading from −1 to −0.09 in the case of nanofiber composites and a similar trend appeared in nanosheet composites. When comparing between nanofiber and nanosheet composites, nanofiber more rapidly increased in terms of slope value. This means that nanofiber is more effective than nanosheet in terms of increasing relaxation time with increasing filler loading. According to these results, we found that nanofiber has a greater effect than nanosheet in the composite in terms of relaxation time because the nanofiber dispersed well in the PS matrix due to its size. However, the nanosheet had large width and length compared with the length of the nanofiber and the flexible nanosheet was able to easily fold or bend in the composite. The slope of the nanofiber composite increased faster than the slope of a nanofiber.

The Cox-Merz relation [33] is used to obtain the shear strain dependence of viscosity from the dynamic viscosity data as follows:

$$\eta(\dot{\gamma})\big|_{\dot{\gamma}=\omega} = \left|\eta^*(\omega)\right| = \sqrt{\eta'^2(\omega) + \eta''^2(\omega)}. \quad (2)$$

Various generalized Newtonian models have been derived by shear viscosity terms in order to analyze the

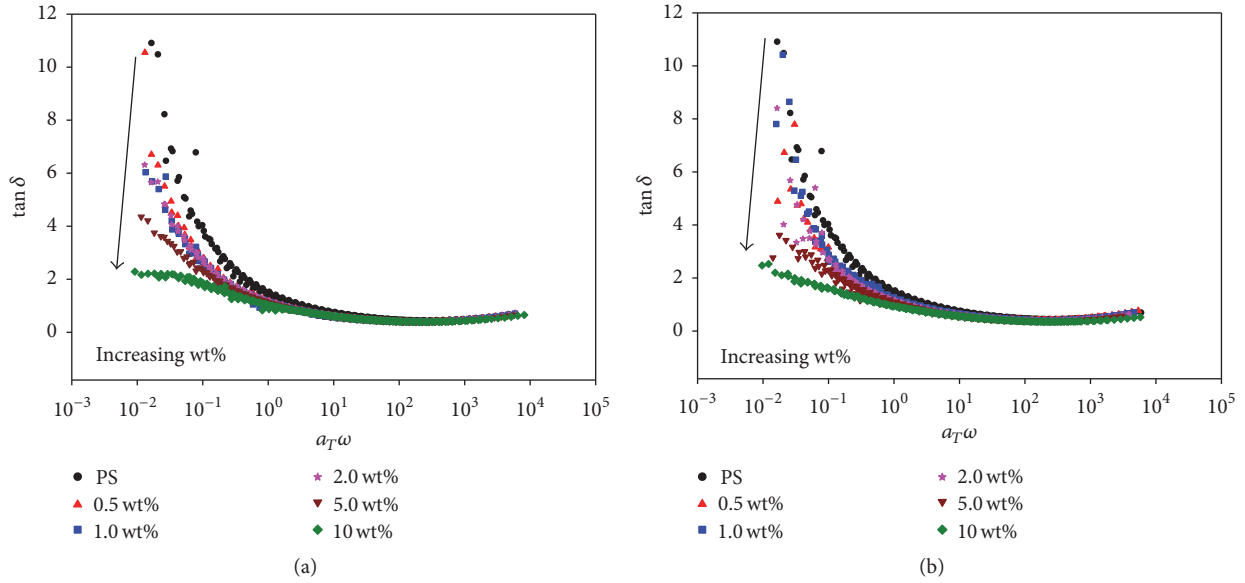

Figure 5: tan δ plot of (a) PS/nanofiber and (b) PS/nanosheet blend in terms of angular frequencies with varying nanofiller loading.

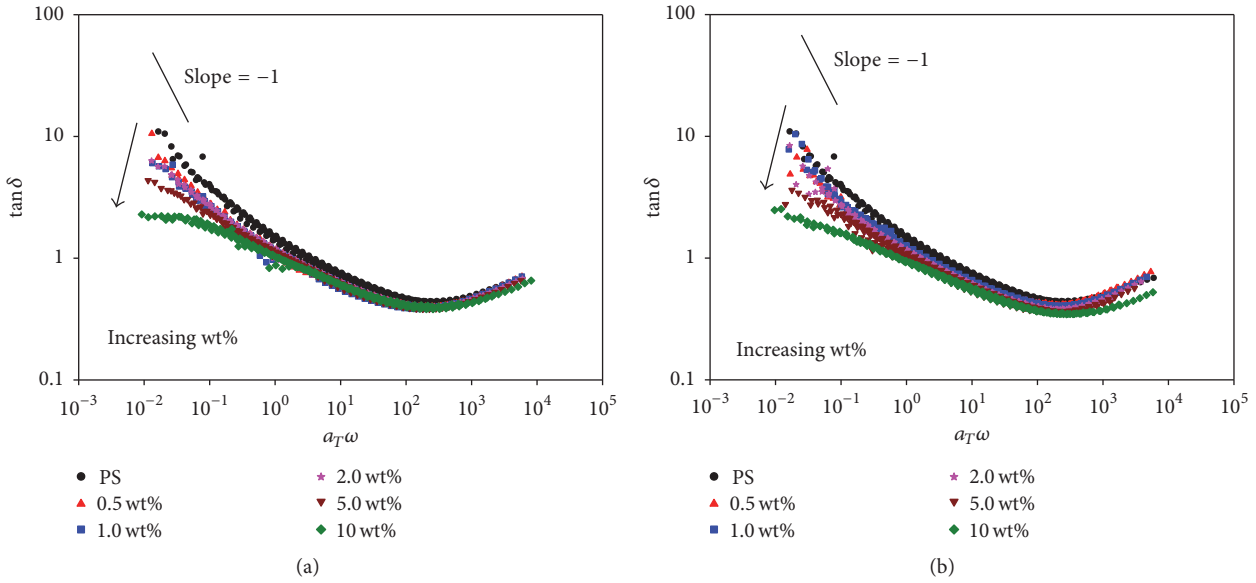

Figure 6: Logarithm tan δ plot of (a) PS/nanofiber and (b) PS/nanosheet blend in terms of angular frequencies with varying nanofiller loading.

viscoelastic properties of polymer composite. The suggested model equation which is Cross-Williamson model [34] involves the terms. This study used this three-parameter model for melt behavior of organic-organic nanocomposites where we found that this model had a good agreement with the experimental results and calculated data compared to other three-parameter models. The model is given by

$$\eta = \frac{\eta_0}{1 + |\lambda\dot{\gamma}|^{1-n}}, \tag{3}$$

where $\eta_0 = \lim_{\dot{\gamma}\to 0}\eta(\dot{\gamma})$ is the zero-shear viscosity, λ is the characteristic time of the composite, and n is the power-law exponent.

Based on the calculation using the Cross-Williamson three-parameter model (Table 3), the zero-shear viscosity and relaxation time values were obtained. Figures 7(a) and 7(b) were plotted using the values in terms of nanofiller content in nanofiber and nanosheet composite. Below 6 wt%, the increasing rate of a nanosheet composite is lower than that of a nanofiber composite. However, after 6 wt% the value of a nanosheet composite is higher than a nanofiber composite.

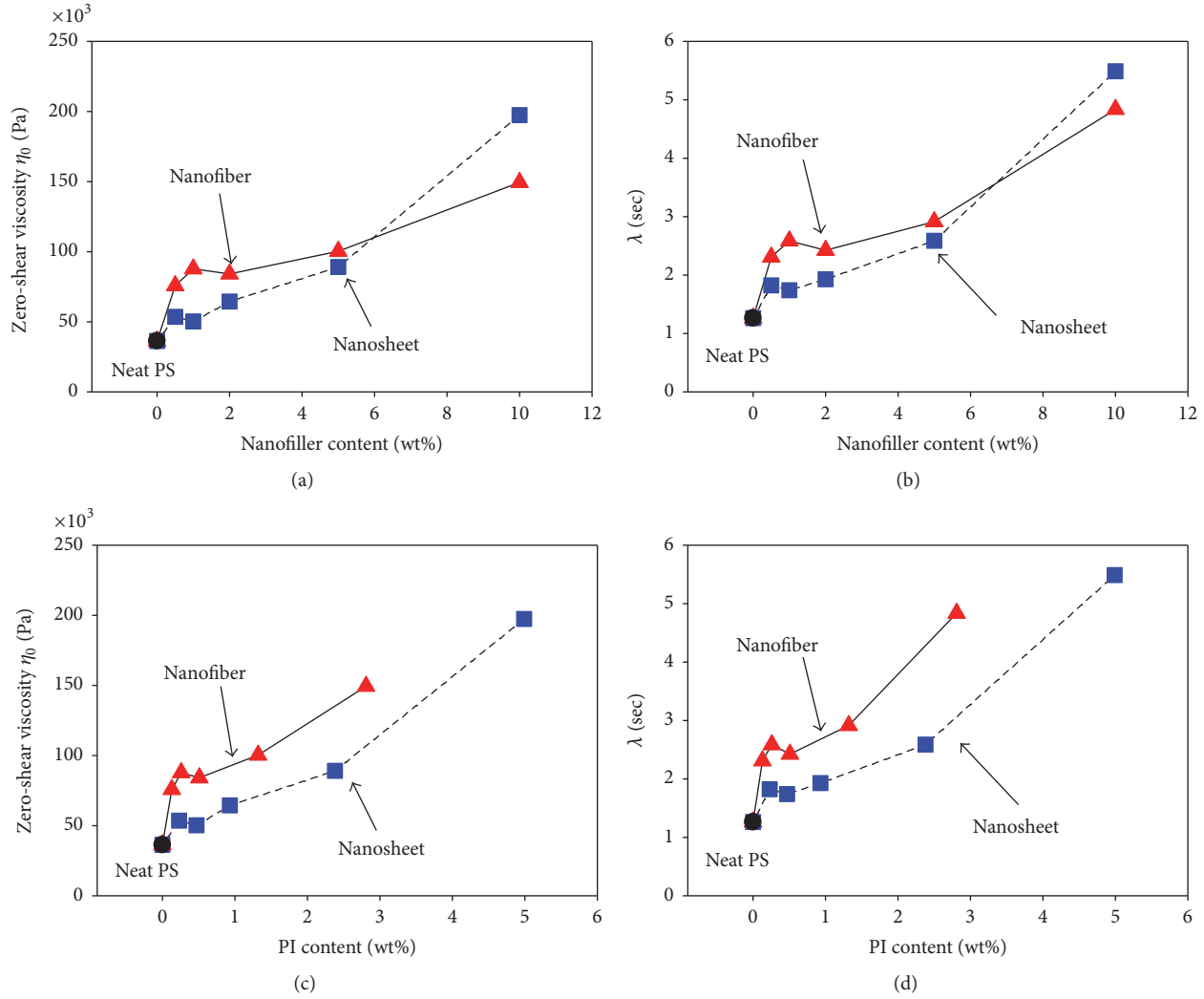

Figure 7: Relaxation time (a) and zero-shear viscosity (b) versus filler content plotted by model fitting data. (c) and (d) are plotted using PI content. Solid line with triangle and dashed line with rectangular indicate PS/nanofiber and PS/nanosheet blend, respectively.

Table 3: Calculated results using Cross-Williamson three-parameter model for zero-shear viscosity, relaxation time, and power-law exponent with neat PS, nanofiber blend, and nanosheet blend with varying nanofiller loading.

Parameters	PS	Nanofiber blend					Nanosheet blend				
		0.5	1.0	2.0	5.0	10.0	0.5	1.0	2.0	5.0	10.0
η_0 (Pa·s)	36,300	75,780	87,800	84,100	100300	149400	53540	50270	64430	89090	197400
λ (sec)	1.262	2.309	2.59	2.424	2.914	4.836	1.8231	1.740	1.929	2.587	5.489
n	0.2678	0.2539	0.2554	0.2582	0.2627	0.2763	0.2382	0.2423	0.2322	0.2327	0.2513

Two values were shown to have a similar tendency. Thus, the rheological model indicated that, in the case of nanosheet composite, structural changes such as continuous domain or aggregation start at above approximately 5 wt%. For comparison with nanofiber and nanosheet in terms of cross-linkable PI content, zero-shear viscosity and relaxation time versus PI content were plotted as shown in Figures 7(c) and 7(d). The values increased without any crossing point which means that the values proportionally increased with PI content. At the same content of PI, the value of nanofiber was higher than the value of nanosheet because nanofiber had good dispersion. In order to study this theoretically, we explored the percolation threshold using a critical volume fraction as follows:

$$1 - \exp\left(-\frac{1.4V}{\langle V_e \rangle}\right) \leq \phi_c \leq 1 - \exp\left(-\frac{2.8V}{\langle V_e \rangle}\right). \quad (4)$$

Generally, the critical volume fraction in blends or composites can be calculated by electrical conductivities using conducting nanofillers to study percolation thresholds.

Researchers have compared these experimental results to simulated results. The critical concentration of nanofibers in a composite is calculated by (4) and had a critical volume faction that was $0.027 \leq \phi_c \leq 0.053$ [35]. According to Balberg [36], critical concentration is related to the total excluded volume, $\langle V_{ex} \rangle$. Excluded volume $\langle V_e \rangle$ in three dimensions can be expressed as

$$\phi_c = 1 - \exp\left(-\frac{\langle V_{ex} \rangle V}{\langle V_e \rangle}\right) = 1 - \exp\left(-N_c V\right), \quad (5)$$

where N_c is the critical number of objects per unit volume. The issues regarding a thin disk that was randomly dispersed in a matrix were studied by Charlaix et al. [37].

$$\langle V_e \rangle = 4\pi r^3 \int_0^{\theta} \sin^2\beta \, d\beta, \quad (6)$$

where β is the angle between the planes of two disks and θ is the angle of the greatest disorientation of the disks. In the randomly oriented disk, $\theta = \pi/2$ was used. Based on (5) and (6), Celzard et al. [35] derived the following equation:

$$1 - \exp\left(-\frac{1.8t}{\pi r}\right) \leq \phi_c \leq 1 - \exp\left(-\frac{2.8t}{\pi r}\right), \quad (7)$$

where t is the thickness of the disks. $\langle V_{ex} \rangle$ of an infinitely thin disk is known to be 1.8 and, for a sphere, 2.8. In our case, the nanosheet had a random shaped sheet, not a regular shaped disk, so we assumed that the nanosheet was disk shape having radius r and a thickness of 70 nm. We also knew that structural change starts from 2 wt% of nanosheet loading. These parameters were used to calculate critical concentration in terms of disk radius.

Based on our assumption, the radius of a nanosheet was around 2-3 μm for the disk by calculating critical concentration in terms of the radius of a nanosheet. However, we only had a range of radius of a nanosheet because the nanosheet shape was quite random and irregular in shape. Thus, the calculated value of critical concentration was $0.013 \leq \phi_c \leq 0.031$. This value overlapped with the critical concentration of nanofiber composite because of the aspect ratio. Thus, we found that the aspect ratio of elastomeric nanoparticles is more related to the percolation threshold than the shape of the nanoparticles.

4. Conclusions

This study presented and compared empirical and theoretical results of elastomeric nanoparticles in terms of particle shape factor by Cole-Cole plot, a Doi-Edward tube model, and a Cross-Williamson model. The shapes of nanofiber and nanosheet filler were formed by a self-assembly technique and cold vulcanization process of PS-PI block copolymers. The rheological behaviors of nanofiber and nanosheet composites were investigated and compared in the melt state in terms of varying frequencies and temperatures. The master curves of two composites indicated that the moduli of nanocomposites increased with increasing nanoparticle content, whereas the moduli of the block copolymer blend (PS/SI23 and PS/SI43) did not have any significant changes. In order to study structural changes, dynamic elasticity coefficient was used to estimate the onset of structural changes in the composite such as with a continuous domain or aggregation. A three-parameter Cross-Williamson model was used to find zero-shear viscosity and relaxation time. A theoretical approach was investigated thru a percolation threshold equation assuming the elastomeric nanoparticles as a rod and disk shape. The calculation indicated that the range of the percolation threshold of nanofiber in a composite was $0.027 \leq \phi_c \leq 0.053$ and the nanosheet was $0.013 \leq \phi_c \leq 0.031$. We confirmed that nanofiber more effectively prevented the motion of matrix PS than nanosheet, rather than being a result of the nanoparticle morphology. Based on these results, we can design conductive nanofiber using multiblock copolymer including conductive core for the application of flexible display and it can replace ITO glass. In addition, it is possible to control gas barrier properties of flexible thin film without decreasing elasticity due to organic nanofiber and nanosheet shape in polymer composites. Nowadays, some of nanofiber research papers are published for various applications such as solar cells [38] and conductive composite membranes [39]. In addition, much attention has been focused on nanosheet research in the field of metal-organic framework [40, 41]. In conclusion, organic nanoparticles shaped nanofiber and nanosheet using block copolymer self-assembly technology and cold vulcanization process can be a promising material for various applications.

Disclosure

Present Address of Sungwon Ma is DuPont Protection Solutions, DuPont Korea Inc., Ulsan 44783, Republic of Korea.

Competing Interests

The authors declare that there are no competing interests regarding the publication of this paper.

References

[1] M. R. Bockstaller, R. A. Mickiewicz, and E. L. Thomas, "Block copolymer nanocomposites: perspectives for tailored functional materials," *Advanced Materials*, vol. 17, no. 11, pp. 1331–1349, 2005.

[2] F. Hussain, M. Hojjati, M. Okamoto, and R. E. Gorga, "Review article: polymer-matrix nanocomposites, processing, manufacturing, and application: an overview," *Journal of Composite Materials*, vol. 40, no. 17, pp. 1511–1575, 2006.

[3] S. Komarneni, "Nanocomposites," *Journal of Materials Chemistry*, vol. 2, no. 12, pp. 1219–1230, 1992.

[4] L. L. Beecroft and C. K. Ober, "Nanocomposite materials for optical applications," *Chemistry of Materials*, vol. 9, no. 6, pp. 1302–1317, 1997.

[5] C. Sanchez, B. Lebeau, F. Chaput, and J.-P. Boilot, "Optical properties of functional hybrid organic-inorganic nanocomposites," *Advanced Materials*, vol. 15, no. 23, pp. 1969–1994, 2003.

[6] K. G. Marra, J. W. Szem, P. N. Kumta, P. A. DiMilla, and L. E. Weiss, "In vitro analysis of biodegradable polymer

blend/hydroxyapatite composites for bone tissue engineering," *Journal of Biomedical Materials Research*, vol. 47, no. 3, pp. 324–335, 1999.

[7] R. Gangopadhyay and A. De, "Conducting polymer nanocomposites: a brief overview," *Chemistry of Materials*, vol. 12, no. 3, pp. 608–622, 2000.

[8] F. Croce, G. B. Appetecchi, L. Persi, and B. Scrosati, "Nanocomposite polymer electrolytes for lithium batteries," *Nature*, vol. 394, no. 6692, pp. 456–458, 1998.

[9] M. Granström and O. Inganäs, "White light emission from a polymer blend light emitting diode," *Applied Physics Letters*, vol. 68, no. 2, pp. 147–149, 1996.

[10] J. N. Coleman, U. Khan, and Y. K. Gun'ko, "Mechanical reinforcement of polymers using carbon nanotubes," *Advanced Materials*, vol. 18, no. 6, pp. 689–706, 2006.

[11] A. J. Crosby and J.-Y. Lee, "Polymer nanocomposites: the 'nano' effect on mechanical properties," *Polymer Reviews*, vol. 47, no. 2, pp. 217–229, 2007.

[12] T. Lan and T. J. Pinnavaia, "Clay-reinforced epoxy nanocomposites," *Chemistry of Materials*, vol. 6, no. 12, pp. 2216–2219, 1994.

[13] K. Y. Lee and L. A. Goettler, "Structure-property relationships in polymer blend nanocomposites," *Polymer Engineering and Science*, vol. 44, no. 6, pp. 1103–1111, 2004.

[14] S. Y. Hobbs, M. E. J. Dekkers, and V. H. Watkins, "Effect of interfacial forces on polymer blend morphologies," *Polymer*, vol. 29, no. 9, pp. 1598–1602, 1988.

[15] B. John, K. T. Varughese, Z. Oommen, P. Pötschke, and S. Thomas, "Dynamic mechanical behavior of high-density polyethylene/ethylene vinyl acetate copolymer blends: the effects of the blend ratio, reactive compatibilization, and dynamic vulcanization," *Journal of Applied Polymer Science*, vol. 87, no. 13, pp. 2083–2099, 2003.

[16] A. F. Yee and R. A. Pearson, "Toughening mechanisms in elastomer-modified epoxies. Part 1. Mechanical studies," *Journal of Materials Science*, vol. 21, no. 7, pp. 2462–2474, 1986.

[17] D. Mangaraj, "Elastomer blends," *Rubber Chemistry and Technology*, vol. 75, no. 3, pp. 365–427, 2002.

[18] R. S. Rajeev and S. K. De, "Thermoplastic elastomers based on waste rubber and plastics," *Rubber Chemistry and Technology*, vol. 77, no. 3, pp. 569–578, 2004.

[19] Y. S. Thio, A. S. Argon, R. E. Cohen, and M. Weinberg, "Toughening of isotactic polypropylene with $CaCO_3$ particles," *Polymer*, vol. 43, no. 13, pp. 3661–3674, 2002.

[20] S. Kumar, M. A. Alam, and J. Y. Murthy, "Effect of percolation on thermal transport in nanotube composites," *Applied Physics Letters*, vol. 90, no. 10, Article ID 104105, 2007.

[21] Y.-H. Ha, Y. Kwon, T. Breiner et al., "An orientationally ordered hierarchical exfoliated clay-block copolymer nanocomposite," *Macromolecules*, vol. 38, no. 12, pp. 5170–5179, 2005.

[22] J. Glazer, "Dilatometric measurement of the rate of vulcanizaton of crêpe-rubber by sulphur monochloride," *Nature*, vol. 167, no. 4245, pp. 404–405, 1951.

[23] G. J. Liu, X. H. Yan, and S. Duncan, "Polystyrene-block-polyisoprene nanofiber fractions. 1. Preparation and static light-scattering study," *Macromolecules*, vol. 35, no. 26, pp. 9788–9793, 2002.

[24] G. Liu, Z. Li, and X. Yan, "Synthesis and characterization of polystyrene-block-polyisoprene nanofibers with different crosslinking densities," *Polymer*, vol. 44, no. 25, pp. 7721–7727, 2003.

[25] C. D. Han, J. Kim, and J. K. Kim, "Determination of the order-disorder transition temperature of block copolymers," *Macromolecules*, vol. 22, no. 1, pp. 383–394, 1989.

[26] M. J. Richardson and N. G. Savill, "Volumetric properties of polystyrene: influence of temperature, molecular weight and thermal treatment," *Polymer*, vol. 18, no. 1, pp. 3–9, 1977.

[27] T. Hashimoto, M. Shibayama, and H. Kawai, "Domain-boundary structure of styrene-isoprene block copolymer films cast from solution. 4. Molecular-weight dependence of lamellar microdomains," *Macromolecules*, vol. 13, no. 5, pp. 1237–1247, 1980.

[28] M. Sepehr, L. A. Utracki, X. X. Zheng, and C. A. Wilkie, "Polystyrenes with macro-intercalated organoclay. Part II. Rheology and mechanical performance," *Polymer*, vol. 46, no. 25, pp. 11569–11581, 2005.

[29] A. Khatory, F. Lequeux, F. Kern, and S. J. Candau, "Linear and nonlinear viscoelasticity of semidilute solutions of wormlike micelles at high salt content," *Langmuir*, vol. 9, no. 6, pp. 1456–1464, 1993.

[30] J. H. Tian, W. Yu, and C. X. Zhou, "The preparation and rheology characterization of long chain branching polypropylene," *Polymer*, vol. 47, no. 23, pp. 7962–7969, 2006, *Polymer*, vol. 48, no. 7, pp. 2186, 2007.

[31] D. Graebling, "Synthesis of branched polypropylene by a reactive extrusion process," *Macromolecules*, vol. 35, no. 12, pp. 4602–4610, 2002.

[32] M. Doi and S. F. Edwards, "Dynamics of concentrated polymer systems. Part 3—the constitutive equation," *Journal of the Chemical Society, Faraday Transactions 2: Molecular and Chemical Physics*, vol. 74, pp. 1818–1832, 1978.

[33] W. P. Cox and E. H. Merz, "Correlation of dynamic and steady flow viscosities," *Journal of Polymer Science*, vol. 28, no. 118, pp. 619–622, 1958.

[34] M. M. Cross, "Rheology of non-Newtonian fluids: a new flow equation for pseudoplastic systems," *Journal of Colloid Science*, vol. 20, no. 5, pp. 417–437, 1965.

[35] A. Celzard, E. McRae, C. Deleuze, M. Dufort, G. Furdin, and J. F. Marêché, "Critical concentration in percolating systems containing a high-aspect-ratio filler," *Physical Review B*, vol. 53, no. 10, pp. 6209–6214, 1996.

[36] I. Balberg, "Excluded-volume explanation of Archie's law," *Physical Review B*, vol. 33, no. 5, pp. 3618–3620, 1986.

[37] E. Charlaix, E. Guyon, and N. Rivier, "A criterion for percolation threshold in a random array of plates," *Solid State Communications*, vol. 50, no. 11, pp. 999–1002, 1984.

[38] M. Nogi, M. Karakawa, N. Komoda, H. Yagyu, and T. T. Nge, "Transparent conductive nanofiber paper for foldable solar cells," *Scientific Reports*, vol. 5, Article ID 17254, 2015.

[39] C. Subramanian, R. A. Weiss, and M. T. Shaw, "Fabrication and characterization of conductive nanofiber-based composite membranes," *Industrial and Engineering Chemistry Research*, vol. 52, no. 43, pp. 15088–15093, 2013.

[40] T. Rodenas, I. Luz, G. Prieto et al., "Metal-organic framework nanosheets in polymer composite materials for gas separation," *Nature Materials*, vol. 14, pp. 48–55, 2015.

[41] Y. Peng, Y. Li, Y. Ban et al., "Metal- organic framework nanosheets as building blocks for molecular sieving membranes," *Science*, vol. 346, no. 6215, pp. 1356–1359, 2014.